Frontiers of Information Technology & Electronic Engineering
www.jzus.zju.edu.cn; engineering.cae.cn; www.springerlink.com
ISSN 2095-9184 (print); ISSN 2095-9230 (online)
E-mail: jzus@zju.edu.cn

Supplementary materials for

Xinying HE, Yuhang LI, Zhuning WANG, Sijie PIAN, Xu LIU, Yaoguang MA, 2024. Recent progress on the applications of micro/nanofibers in ultrafast optics. *Front Inform Technol Electron Eng*, 25(9):1193-1208. https://doi.org/10.1631/FITEE.2300509

1 Theoretical analysis of mode evolution of MNFs

In the taper transition region, the alteration of geometric parameters disrupts the inherent orthogonality of the modes, resulting in mode coupling. As a consequence, the exact field within this region can be expressed as (Snyder and Love, 1984)

$$\frac{\mathrm{d}b_k(z)}{\mathrm{d}z} - i\beta_k(z)b_k(z) = \sum_{j\neq k} C_{jk}(z)b_j(z), \tag{S1}$$

where b_k is the complex amplitude. The coupling coefficient C_{jk} is given by (Snyder and Love, 1984; Digonnet et al., 2001)

$$C_{jk} = \frac{k}{4}\left(\frac{\varepsilon_0}{\mu_0}\right)^{\frac{1}{2}} \frac{1}{\beta_j-\beta_k}\int_{A_\infty} \hat{e}_j^* \cdot \hat{e}_k \cdot \frac{\partial n^2}{\partial z}\mathrm{d}A\ (j\neq k) = \frac{k}{4}\left(\frac{\varepsilon_0}{\mu_0}\right)^{\frac{1}{2}} \frac{1}{\beta_j-\beta_k}\int_{A_\infty} \hat{e}_j^* \cdot \hat{e}_k \cdot \frac{\partial n^2}{\partial r}\frac{dr}{\mathrm{d}z}\mathrm{d}A\ (j\neq k), \tag{S2}$$

where $\hat{e}_j$ and $\hat{e}_k$ are the normalized mode fields of two different modes, n represents the spatial distribution of the refractive index, and A_∞ represents the infinite cross-section.

When the taper is steep (i.e., $\frac{\mathrm{d}r}{\mathrm{d}z}$ is large), the effective refractive index of the fundamental mode decreases along the taper, approaching that of the cladding. Consequently, the fundamental mode gradually leaks out and becomes guided by the cladding-to-air interface. Given a larger difference in refractive index between the new cladding and the new core, the condition required for single-mode transmission cannot be met, and an exchange of power commences between the fundamental mode and the higher-order modes (Fig. S1a) (Siyu Chen, 2019). When the coupling coefficient obtained from Eq. (S2) is very small, there is no obvious power transfer in the propagation process. This is referred to as the adiabatic regime (Snyder and Love, 1984).

According to Eqs.(S1) and (S2), the mode field distribution of different coupling modes at any position along the taper can be obtained (Leng and Yam, 2019; Siyu Chen, 2019; Zhou et al., 2022). The transmission characteristics can be customized by controlling the shape of the taper.

The waist region of the MNF features a uniform diameter distribution where the new cladding layer is just air or another additional coating. The optical properties of the waist region can be analyzed with the Helmholtz equation similar to traditional optical fibers. As illustrated in Fig. S1b, as the fiber radius decreases, most of the higher-order modes are cut off, with only a subset of the lower-order modes being capable of persisting.

The biconical MNFs with intermodal interference engender oscillating transmission spectra, endowing these fibers an exceptional ability to serve as an effective wavelength selection component in mode-locked wavelength-tunable fiber lasers (Fang et al., 2010; Dai et al., 2023).

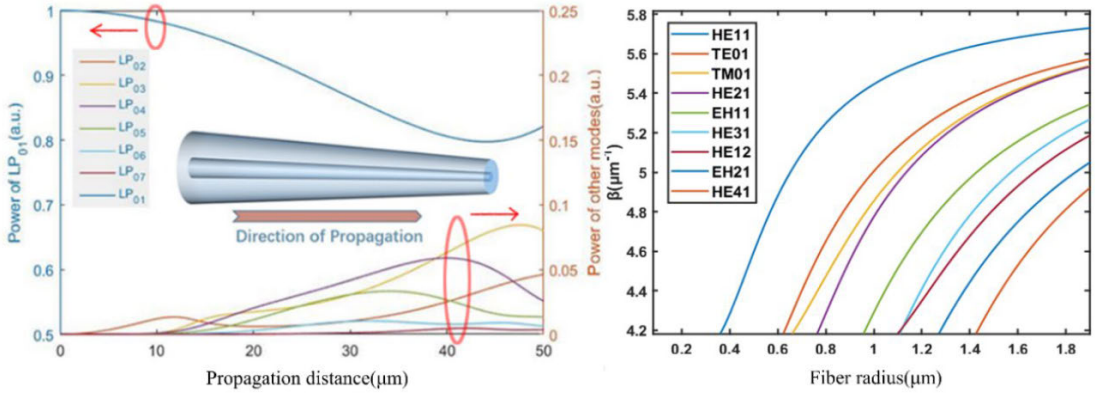

(a) (b)

Fig. S1 Mode evolution and properties of MNFs: (a) the power of different modes varying along the taper (Siyu Chen, 2019); (b) diameter-dependent propagation constant of different modes of MNFs

2 Theory of dispersion characteristics of MNFs

The dispersion properties of MNFs can be characterized by the waveguide dispersion $D_w = \frac{\mathrm{d}(\beta_1)}{\mathrm{d}\lambda} = -\frac{2\pi c}{\lambda^2}\beta_2$, where β_1 and β_2 are the first and second derivatives of β, respectively. The expression for β_1 can be represented as (Snyder and Love, 1984)

$$\beta_1 = {v_g}^{-1} = \left(\frac{c}{{n_1}^2}\cdot\frac{\beta}{k}\cdot\frac{1}{1-2\Delta\eta}\right)^{-1}, \tag{S3}$$

where η is the proportion of the evanescent field and Δ is a parameter describing the relative refractive index difference between the core and the cladding. The waveguide dispersion D_w is related to η, which is significantly affected by the diameter. This relationship suggests that diameter directly impacts waveguide dispersion.

Different materials exhibit a variety of refractive index distributions, resulting in different mode field distributions and dispersion characteristics. The structure and cross-section shape influence the mode field distribution and subsequently affect the dispersion. Triangular and hexagonal nanowires exhibit some deviation in the mode field distribution compared to cylindrical fibers and this inevitably affects the dispersion distribution (Ma et al., 2013). For PCFs, the influence of structural parameters (air hole diameter and pitch) on dispersion has been extensively studied (Mogilevtsev et al., 1998). Flat dispersion and a tunable zero-dispersion wavelength can be achieved by adjusting these structural parameters (Medjouri et al., 2015; Stepniewski et al., 2018; Sultana et al., 2018; Thi et al., 2022).

3 Other characteristics of MNFs

MNFs obtained from traditional fibers have fiber tails at both ends, allowing them to be spliced with standard optical fibers and easily connected to other fibers and fiberized components (Brambilla, 2010). As a result, they offer low insertion loss capability. A typical value for insertion loss is 0.1 dB (Brambilla et al., 2009). In the case of polymer and semiconductor nanowires, their diameters often differ considerably from standard optical fibers. The smaller diameters of these materials make it challenging to achieve precise alignment with traditional fibers, resulting in a larger mismatch and increased insertion loss. Transmission loss usually results

from radiation (e.g., scattering from the structural nonuniformity) and absorption. Generally, as the diameter decreases, the transmission loss of an optical fiber increases. This is primarily due to the increased proportion of evanescent wave propagation and the susceptibility to scattering caused by surface contamination (Tong et al., 2003). The impact of different surface roughness on transmission loss has been extensively studied (Kovalenko et al., 2008; Brambilla, 2010). For MNFs obtained from traditional fiber tapering, it is feasible to achieve high transmission efficiency by suppressing the energy transfer in the taper region (i.e., adiabaticity) and minimizing scattering losses in the waist region. The transmittance of an MNF with a waist diameter of 1.2 μm and a length of 10 cm can reach 99.4%. As the diameter decreases, the ultimate transmittance is limited by the intrinsic scattering loss. Propagation loss is estimated as 5.5×10^{-4} dB/mm for an MNF with a diameter of 0.8 μm (Yao et al., 2020). Compared with the MNFs obtained from a traditional optical fiber, a polymer nanowire usually has higher nonuniformity and consequently a higher optical loss. Significant advancements have been made in achieving low transmission losses in polymer fibers. The loss in a polystyrene/quantum dot nanowire with a diameter of 560 nm can be as low as 0.1-0.2 dB/mm (Gu et al., 2008; Meng et al., 2011).

The high mechanical strength and compatibility of conventional optical fibers are also reasons why MNFs have potential applications in ultrafast optics. These features make MNFs well suited for coating and fabrication of all-fiber structures in ultrafast optics.

4 Some comparison results from supercontinuum generation

Table S1 summaries comparisons of SC generation using diverse types of optical fibers. However, the exploration of SC phenomena extends far beyond the confines of our summary, as doped fibers or highly nonlinear material fibers have been extensively harnessed to augment the pertinent spectral characteristics (Li et al., 2019; Niang et al., 2019; Saini et al., 2019). For the sake of comparative analysis, our focus is primarily on silica fibers that have been instrumental in yielding SC spectra. Within this context, it is evident that the implementation of tapering techniques has greatly enhanced the efficacy of the SC generation process, offering an increased spectral width per unit of power and length. While the tapered multimode fibers may not exclusively exhibit the highest magnitudes of this performance metric, their overall spectral uniformity has been meticulously optimized, thus heralding a significant advancement in this field.

Table S1 Comparison of supercontinuum generated by different optical fibers

Fiber type	Pump parameter	Peak power (kW)	Fiber length (cm)	Spectral range (nm)	Spectral width (nm/(cm·kW))	reference
Uniform PCF	100 fs, 790 nm	8	75	390-1600	2.016	Ranka et al. (2000)
	100 fs, 780 nm	3	100	450-1250	2.667	Dudley et al. (2002)
Tapered PCF	39 fs, 523 nm	10	10	400-750	3.5	Stark et al. (2010)
	130 fs, 800 nm	38.462	1.7	293-1650	20.754	Stark et al. (2012)
Uniform MNF	350 fs, 850 nm	11.142	9	370-1545	11.717	Birks et al. (2000)
	350 fs, 850 nm	6.766	25	300-1800	8.867	Man et al. (2001)
Tapered MNF	400 ps, 1064 nm	300	50	450-2400	0.13	Eftekhar et al. (2019)

References

Birks TA, Wadsworth WJ, Russell PS, 2000. Supercontinuum generation in tapered fibers. *Opt Lett*, 25(19):1415-1417. https://doi.org/10.1364/OL.25.001415

Brambilla G, 2010. Optical fibre nanowires and microwires: a review. *J Optics*, 12(4):043001. https://doi.org/10.1088/2040-8978/12/4/043001

Brambilla G, Xu F, Horak P, et al., 2009. Optical fiber nanowires and microwires: fabrication and applications. *Adv Optics Photon*, 1(1). https://doi.org/10.1364/aop.1.000107

Dai L, Huang Z, Huang Q, et al., 2023. Microfiber assisted bidirectional wavelength-locked ultrafast erbium-doped fiber laser. *Optics & Laser Technology*, 162:109219. https://doi.org/10.1016/j.optlastec.2023.109219

Digonnet MJF, Daxhelet X, Gonthier F, et al., 2001. Optical properties of tapered fiber filters for telecommunication applications. Optical Devices for Fiber Communication II, p.67-77. https://doi.org/10.1117/12.414122

Dudley JM, Provino L, Grossard N, et al., 2002. Supercontinuum generation in air–silica microstructured fibers with nanosecond and femtosecond pulse pumping. *J Opt Soc Amer B*, 19(4). https://doi.org/10.1364/josab.19.000765

Eftekhar MA, Sanjabi-Eznaveh Z, Lopez-Aviles HE, et al., 2019. Accelerated nonlinear interactions in graded-index multimode fibers. *Nat Commun*, 10(1):1638. https://doi.org/10.1038/s41467-019-09687-9

Fang Q, Kieu K, Peyghambarian N, 2010. An all-fiber 2 μm wavelength-tunable mode-locked laser. *IEEE Photon Technol Lett*, 22(22):1656-1658. https://doi.org/10.1109/lpt.2010.2077736

Gu F, Zhang L, Yin X, et al., 2008. Polymer single-nanowire optical sensors. *Nano Lett*, 8(9):2757-2761. https://doi.org/10.1021/nl8012314

Kovalenko AV, Kurashov VN, Kisil AV, 2008. Radiation losses in optical nanofibers with random rough surface. *Opt Express*, 16(8):5797-5806. https://doi.org/10.1364/oe.16.005797

Leng X, Yam SSH, 2019. Analytical model for abrupt tapered Mach–Zehnder interferometer based on coupled mode theory. *IEEE Photon Technol Lett*, 31(19):1600-1603. https://doi.org/10.1109/lpt.2019.2939949

Li G, Peng X, Dai S, et al., 2019. Highly coherent 1.5–8.3 μm broadband supercontinuum generation in tapered As–S chalcogenide fibers. *J Lightw Technol*, 37(9):1847-1852. https://doi.org/10.1109/jlt.2018.2876692

Ma Y, Guo X, Wu X, et al., 2013. Semiconductor nanowire lasers. *Adv Optics Photon*, 5(3):216-273. https://doi.org/10.1364/aop.5.000216

Man TPM, Birks TA, Wadsworth WJ, et al., 2001. Fabrication of indefinitely long tapered fibres for supercontinuum generation. *Nonl Guid Wave Appl*, Article WB4. https://doi.org/10.1364/NLGW.2001.WB4

Medjouri A, Simohamed LM, Ziane O, et al., 2015. Design of a circular photonic crystal fiber with flattened chromatic dispersion using a defected core and selectively reduced air holes: application to supercontinuum generation at 1.55 μm. *Photon Nanost Fund Appl*, 16:43-50. https://doi.org/10.1016/j.photonics.2015.08.004

Meng C, Xiao Y, Wang P, et al., 2011. Quantum-dot-doped polymer nanofibers for optical sensing. *Adv Mater*, 23(33):3770-3774. https://doi.org/10.1002/adma.201101392

Mogilevtsev D, Birks TA, Russell PS, 1998. Group-velocity dispersion in photonic crystal fibers. *Opt Lett*, 23(21):1662-1664. https://doi.org/10.1364/ol.23.001662

Niang A, Mansuryan T, Krupa K, et al., 2019. Spatial beam self-cleaning and supercontinuum generation with Yb-doped multimode graded-index fiber taper based on accelerating self-imaging and dissipative landscape. *Opt Express*, 27(17):24018-24028. https://doi.org/10.1364/OE.27.024018

Ranka JK, Windeler RS, Stentz AJ, 2000. Visible continuum generation in air-silica microstructure optical fibers with anomalous dispersion at 800 nm. *Opt Lett*, 25(1):25-27. https://doi.org/10.1364/ol.25.000025

Saini TS, Trung Hoa NP, Tuan TH, et al., 2019. Tapered tellurite step-index optical fiber for coherent near-to-mid-IR supercontinuum generation: experiment and modeling. *Appl Opt*, 58(2):415-421. https://doi.org/10.1364/AO.58.000415

Siyu Chen HG, Wang Z, Liu YG, 2019. Mode transmission analysis of tapered fiber based on coupled local mode theory. Asia Communications and Photonics Conf.

Snyder AW, Love JD, 1984. Optical Waveguide Theory. Springer New York, NY, USA.

Stark SP, Podlipensky A, Joly NY, et al., 2010. Ultraviolet-enhanced supercontinuum generation in tapered photonic crystal fiber. *J Opt Soc Amer B*, 27(3). https://doi.org/10.1364/josab.27.000592

Stark SP, Travers JC, Russell PS, 2012. Extreme supercontinuum generation to the deep UV. *Opt Lett*, 37(5):770-772. https://doi.org/10.1364/OL.37.000770

Stepniewski G, Pniewski J, Pysz D, et al., 2018. Development of dispersion-optimized photonic crystal fibers based on heavy metal oxide glasses for broadband infrared supercontinuum generation with fiber lasers. *Sensors*, 18(12):4127. https://doi.org/10.3390/s18124127

Sultana J, Islam MS, Islam MR, et al., 2018. High numerical aperture, highly birefringent novel photonic crystal fibre for medical imaging applications. *Electron Lett*, 54(2):61-62. https://doi.org/10.1049/el.2017.3694

Thi TN, Trong DH, Van LC, 2022. Supercontinuum generation in ultra-flattened near-zero dispersion PCF with C_7H_8 infiltration. *Opt Quant Electron*, 55(1):93. https://doi.org/10.1007/s11082-022-04351-x

Tong L, Gattass RR, Ashcom JB, et al., 2003. Subwavelength-diameter silica wires for low-loss optical wave guiding. *Nature*, 426(6968):816-819. https://doi.org/10.1038/nature02193

Yao N, Linghu S, Xu Y, et al., 2020. Ultra-long subwavelength micro/nanofibers with low loss. *IEEE Photon Technol Lett*, 32(17):1069-1072. https://doi.org/10.1109/lpt.2020.3011719

Zhou X, Chen Z, Wang Y, et al., 2022. Theoretical analysis of mode evolution in an adiabatically tapered multimode fiber by coupled local mode theory. *Opt Fiber Technol*, 70:102898. https://doi.org/10.1016/j.yofte.2022.102898